J. Fluid Mech. (2001), *vol.* 426, *pp.* 73–94. Printed in the United Kingdom

Leading-edge receptivity of a hypersonic boundary layer on a flat plate

By A. A. MASLOV[1], A. N. SHIPLYUK[1], A. A. SIDORENKO[1] AND D. ARNAL[2]

[1]Institute of Theoretical and Applied Mechanics, Russian Academy of Sciences, Novosibirsk, 630090, Russia

[2]CERT, ONERA, Toulouse, France

(Received 5 November 1998 and in revised form 23 August 2000)

Experimental investigations of the boundary layer receptivity, on the sharp leading edge of a flat plate, to acoustic waves induced by two-dimensional and three-dimensional perturbers, have been performed for a free-stream Mach number $M_\infty = 5.92$. The fields of controlled free-stream disturbances were studied. It was shown that two-dimensional and three-dimensional perturbers radiate acoustic waves and that these perturbers present a set of harmonic motionless sources and moving sources with constant amplitude. The disturbances excited in the boundary layer were measured. It was found that acoustic waves impinging on the leading edge generate Tollmien–Schlichting waves in the boundary layer. The receptivity coefficients were obtained for several radiation conditions and intensities. It was shown that there is a dependence of receptivity coefficients on the wave inclination angles.

1. Introduction

The subject of laminar–turbulent transition is of considerable practical interest and has a wide range of engineering applications, due to the fact that transition controls the evolution of important aerodynamic quantities such as drag or heat transfer. In particular, the heating rates generated by a turbulent boundary layer may be several times higher than those for a laminar boundary layer, and so the prediction of transition is of great practical importance for hypersonic vehicles.

The mechanisms that drive the dynamics of the transition to turbulence depend on the environmental disturbance level. If the free-stream disturbances are weak enough and the wall is smooth, the first stage of the transition process is the so-called boundary layer *receptivity* (Morkovin 1969). Receptivity refers to the mechanism by which the environmental disturbances enter the boundary layer and generate unstable waves. The linear amplification of these waves constitutes the second step of the transition process, and it can be described by the linear stability theory. The third stage occurs when unstable waves reach a finite amplitude. Their behaviour begins to deviate from that predicted by the linear theory, and this nonlinear evolution eventually results in the breakdown to turbulence.

At the present time, the receptivity mechanisms are poorly understood, especially at high Mach numbers. However, the understanding of these phenomena is of great importance because the receptivity links the amplitude of the free-stream disturbances and the initial amplitude of the unstable waves. If the 'transformation coefficient' is known, the amplification criteria for transition prediction (for instance the e^n method)

can be replaced by amplitude criteria that are more relevant from the physical point of view.

The majority of theoretical and experimental studies of receptivity have been performed for subsonic flow velocities. Reviews on this topic can be found in Nishioka & Morkovin (1986), Kerschen (1989), Goldstein & Hultgren (1989) and Kozlov & Ryzhov (1990).

Receptivity investigations at super- and hypersonic flow velocities are more complicated and have not been performed in detail. The first attempt at theoretical investigation of the interaction of acoustic waves with a supersonic boundary layer on the basis of the linear stability theory was made by Mack (1975). It was found that external acoustic waves induce growing pulsations in the boundary layer; their amplitude exceeds the amplitude of external acoustic waves by several times. Similar research was also carried out by Gaponov (1977).

The interaction of free-stream disturbances with shock waves may be regarded as a step in the receptivity process. It was shown (McKenzie & Westphal 1968) that a single entropy, acoustic or vorticity wave upstream of the shock produces a disturbance comprising a mixture of all three classes downstream of the shock. Duck, Lasseigne & Hussaini (1997) found that the weak shock solution is stable to all classes of three-dimensional free-stream disturbances.

The generation of instability waves in regions of local wall inhomogeneities was examined theoretically in Choudhari & Streett (1990). It was found that receptivity to acoustic free-stream disturbances is much stronger than to vortical or entropy type free-stream disturbances and appears to be more sensitive to the direction of the incident radiation.

Excitation of first and second mode disturbances near a sharp leading edge of a flat plate by three-dimensional acoustic waves was analysed in an asymptotic approximation by Fedorov & Khohlov (1993). Two mechanisms of disturbance excitation were distinguished in this work. The first mechanism was associated with diffraction of the incident and reflected acoustic waves; the second one was related to scattering of the incident wave on the leading edge of the plate, which is equivalent to the emergence of a cylindrical source of sound on it. It follows that the generation of disturbances in the boundary layer depends on the angle of incidence of acoustic waves onto the plate and on the direction of incidence of these waves (from above or from below). The excitation of disturbances in the boundary layer by a streamwise acoustic field was studied by Gaponov (1995). A strong dependence of disturbance intensity in the boundary layer on the spatial orientation of external acoustic waves was obtained.

Results of the direct numerical simulation of the generation of boundary layer instability waves due to free-stream acoustic disturbances for a two-dimensional flow over a parabola at free-stream Mach number $M_\infty = 15$ were presented in Zhong (1997). It was shown that external disturbances generate instability waves mainly in the leading-edge region and that these waves contain both the first and second mode of instabilities.

The effect of different external disturbances on Mach 8 flow past a sharp wedge was studied by Malik, Lin & Sengupta (1999). External harmonic disturbances were introduced through suction/blowing, Mach waves and plane acoustic wave. It was found that two modes of instability with phase velocities $C = 1 - 1/M$ and $C = 1 + 1/M$ were excited and the slow mode eventually grew to large amplitude.

The first experimental study of boundary layer receptivity to external disturbances at supersonic flow velocities was carried out by Kendall (1975). The evolution of natural disturbances in the boundary layer was studied and the correlation coefficients

between the free stream and boundary layer pulsations were measured. The external acoustic field was found to induce pulsations of higher intensity in the boundary layer near the leading edge of the plate. Temporal correlation measurements were performed at Mach numbers $M_\infty = 1.6$–5.6 and showed that the correlation coefficients are growing with increase of the Mach number. Spatial correlation measurements were carried out at Mach number $M_\infty = 4.5$ and showed that inclined waves have the maximum correlation coefficients.

Detailed information about the receptivity process can be obtained only by carrying out experiments in controlled conditions using artificial disturbances. A repeatable, localized, laser-generated perturbation technique was developed by Schmisseur, Schneider & Collicott (1998) for application to supersonic and hypersonic boundary layer receptivity measurements.

A method using controlled disturbances has been developed at ITAM SB RAS to study the wave processes in supersonic flows (Kosinov, Maslov & Shevelkov 1990). It was found in Maslov & Semionov (1986, 1987) that the most intensive generation of natural pulsations of the boundary layer by acoustic waves takes place at the leading edge, at the lower branch of the neutral curve and in the region of the maximum amplification of external acoustic disturbances by the supersonic boundary layer. Experimental data on the amplification of external acoustic disturbances were in qualitative agreement with the theoretical calculations (Mack 1975; Gaponov 1977).

The wave structure of the boundary layer disturbances induced by acoustic waves incident onto the leading edge of a flat plate from above was studied. The data obtained were compared with the wave structure of disturbances excited by a local source in the boundary layer. The results revealed a complicated structure of the transformation of external acoustic waves to disturbances of the boundary layer.

When acoustic waves fell on the model from above, the boundary layer pulsations were excited in each of the three regions of receptivity simultaneously (Maslov & Semionov 1986, 1987), and it was extremely difficult to distinguish the receptivity of each region. The technique of receptivity research has been modified recently. When acoustic waves are coming from below, only one region of receptivity is left, namely, the leading edge. Using the acoustic waves incident onto the leading edge of the model from below, receptivity studies were performed at Mach numbers $M_\infty = 2$ (Semionov, Kosinov & Maslov 1996) and $M_\infty = 3.5$ (Kosinov, Maslov & Semionov 1996). It was found in Semionov *et al.* (1996), that receptivity coefficients depend on the longitudinal phase velocity C and inclination angle of external acoustic waves χ.

The field of controlled disturbances in the free stream at $M_\infty = 3.5$ was studied in Kosinov *et al.* (1996). The field of disturbances had a more complicated structure than at $M_\infty = 2$. The absolute amplitudes and the mode structure of controlled pulsations were determined. It was shown that disturbances introduced into the free stream had an acoustic nature. The excitation of pulsations in the boundary layer by external disturbances at $M_\infty = 3.5$ was much more intensive than at $M_\infty = 2$. Inclined waves had higher receptivity level than the waves with $\chi = 0^\circ$.

In the present paper the first experimental study of receptivity at hypersonic flow velocities is performed. The receptivity at the leading edge of a flat-plate boundary layer to external acoustic disturbances in the incoming flow is investigated using controlled disturbances. Two- and three-dimensional perturbers are used for generating these disturbances. Note that studies of waves with zero inclination angle ($\chi = 0^\circ$) are very important at hypersonic speeds because the second-mode waves, that are most unstable at high Mach numbers, have $\chi = 0^\circ$, too.

Boundary layer stability is extremely sensitive to small perturbation and its study

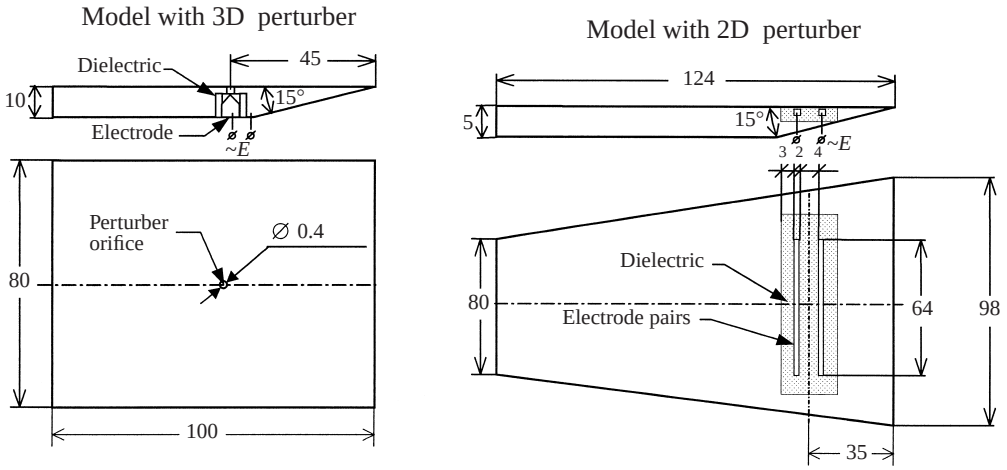

FIGURE 1. Schematics of the models with disturbance sources. Dimensions are in mm.

M_∞	P_0	T_0	Re_1	f	F
5.92	1.08 MPa	390 K	13×10^6 m^{-1}	50 kHz	0.30×10^{-4}

TABLE 1. Main experimental parameters.

demand very careful and detailed measurements. A list of requirements for low-speed stability experiments, that must be satisfied in order to be able to successfully interpret results obtained, is given in Saric (1990). Unfortunately there are still no such requirements for high-speed experiments and so standard rules are used: (1) the linear problem must be correct and (2) initial conditions must be provided for theory and computations (see Saric 1990).

2. Experimental apparatus

2.1. *Wind tunnel and models*

The experiments are conducted in the hypersonic blow-down wind tunnel T-326 with open-jet test section at the Institute of Theoretical and Applied Mechanics of Siberian Branch of Russian Academy of Sciences in Novosibirsk (ITAM RAS) (Grigoriev *et al.* 1972). The diameter of the axisymmetric contoured nozzle is 200 mm. The time of continuous operation of the wind tunnel is up to 1200 s. The Mach number flow field non-uniformity in the flow core at $M_\infty \approx 6$ is 0.7%. The diameter of the test core is about 180 mm. The noise level is about 1%. This value is common for conventional supersonic wind tunnels. The main experimental parameters are given in table 1. During the experiment pressure P_0 and temperature T_0 are kept constant with the maximum possible accuracy. The results of hot-wire measurements show that the mass flow in the free stream ($\rho_\infty U_\infty$), where ρ is density and U flow velocity, varies in the course of experiment by no more than 1%. The model walls are at adiabatic conditions.

Three models are used for the experiments: a model with a two-dimensional perturber, a model with a three-dimensional perturber, and a test model (figure 1). All the models are flat steel plates with sharp leading and side edges. The radius of the

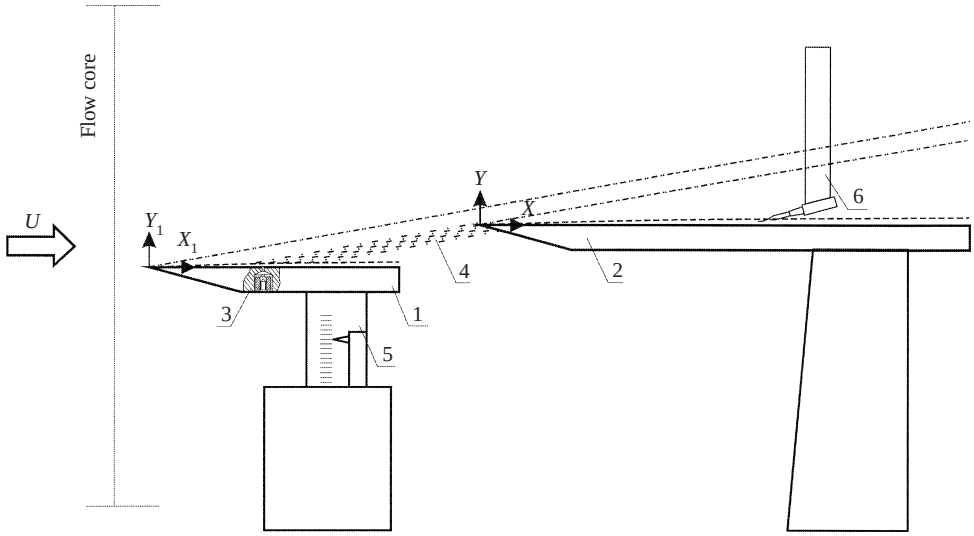

FIGURE 2. The model disposition in the test section: 1 – model with two-dimensional or three-dimensional perturber, 2 – test model, 3 – source of disturbances, 4 – acoustic radiation, 5 – model pylon, 6 – hot wire.

leading edges of the models is less than 0.05 mm. The surface roughness is 0.6 μm. The construction of the three-dimensional perturber is based on a glow electric discharge in the chamber and is similar to the construction described in Kosinov *et al.* (1990). Artificial disturbances are introduced into a hypersonic boundary layer through an orifice 0.4 mm in diameter in the working surface of the plate.

The model with a two-dimensional perturber is equipped with a source of two-dimensional disturbances (figure 1). The construction of this perturber is similar to the construction used by Kendall (1967). It contains two long copper electrodes which are located parallel to the leading edge on the model surface and are separated by a dielectric. This construction allows one to obtain a linear glow discharge uniformly distributed over the entire length of the electrodes.

The test model was designed to study the receptivity to external controlled disturbances. The main dimensions of the plate are as follows: length 195 mm, leading-edge width 120 mm, base width 100 mm, thickness 10 mm. A schematic of the model positions in the test section is shown in figure 2. The test model is mounted on a pylon at the flow centreline and is located in the region of influence of disturbances from the models with two-dimensional or three-dimensional perturbers, which are mounted on another pylon. It is possible to move the models in the vertical direction between the runs. The models are installed at zero incidence with an accuracy of 0.3°. The X distance between the leading edges of the model with a two-dimensional perturber and the test model is $\Delta X = 99$ mm, that between the model with a three-dimensional perturber and the test model is 132.5 mm. The Y distance between the models is chosen after the field of disturbances in the free stream is investigated.

2.2. *Measuring system*

To determine the flow parameters, the pressure P_0 and temperature T_0 in the settling chamber are measured. The pressure P_0 is measured by a pressure strain gauge with an accuracy of 0.5%. The temperature T_0 is measured by a thermocouple with an accuracy of 0.5%.

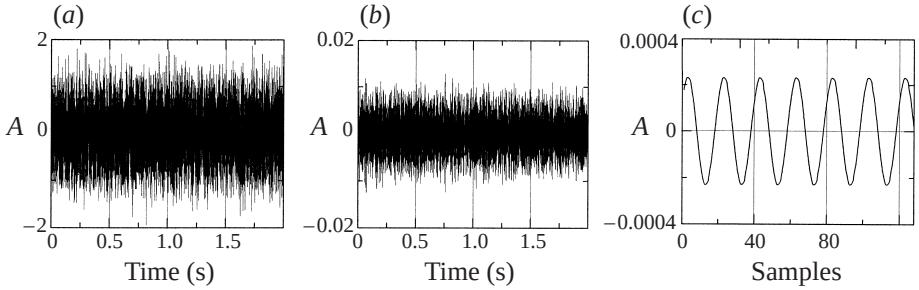

FIGURE 3. Sample time-traces. (*a*) Input signal, (*b*) amplifier with 1% transmission band output, (*c*) phase-locked ensemble-averaging.

Two traverse gears are used for moving the hot-wire probe: a three-component traverse gear for moving the probes in the X, Y, Z directions with an accuracy of 0.1 mm; and a one-component microtraverse gear for boundary layer measurements with a displacement accuracy of 0.01 mm.

A constant-temperature hot-wire anemometer custom built at ITAM is used to measure the mass flow fluctuations. The hot-wire probes are made of tungsten wire 5 μm in diameter and 1 mm long, which is welded to pointed stings. The overheat ratio is 0.38–0.42. The frequency response of the hot-wire anemometer is about 400 kHz. An alternate signal from the hot wire is fed to a selective amplifier with a 1% transmission bandwidth tuned to the frequency of the introduced pulsations, thus improving the signal-to-noise ratio. The 1% transmission band equals the averaging of 100 cycles of pulsations. The constant and alternate components of the hot-wire signal are measured by a two-channel 10-bit ADC with a sampling frequency of 1 MHz. To exclude random fluctuations and reveal artificial disturbances, a phase-locked ensemble averaging of time series is used. For this purpose, the recorded time-series of 128 samples are summed 1000 times. Some sample time-traces are shown in figure 3. A great improvement in signal/noise ratio is seen after using this technique.

To generate a high-frequency discharge, an electric pulse generator is used. It generates high-voltage (up to 1000 V) electric pulses with duration of 2 μs and repetition frequency of 30–180 kHz. This device is triggered by a master frequency generator with a frequency stability better than 0.01% and is fed from a DC source. The feed current is measured by a digital voltmeter. For a synchronous summation of the alternate hot-wire signal, the ADC is triggered simultaneously with the discharge ignition. For this purpose, the signal from the master generator is supplied to the ADC synchronization input.

3. Data processing

It is assumed in data processing that at a high overheating the hot wire is sensitive only to mass-flow fluctuations, since the mass-flow fluctuations are much larger than the temperature fluctuations. The mass-flow sensitivity factor L is practically independent of the Reynolds number and hot-wire probe overheating for the constant-temperature anemometer (Bestion, Gaviglio & Bonnet 1983). Its value can be found from the heat transfer law suggested by Kovasznay (1954), which yields $L \approx n/2$ (n is the power of the Reynolds number in the function $Nu(Re)$). At low Reynolds numbers (Re) the value of L changes at small overheating. It was shown in Bestion

et al. (1983) that in the case of large overheating ($a_w \geqslant 0.4$) this effect can be ignored. The sensitivity coefficient is changed by less than 0.01 for $Re_w = 6.4$ and $a_w = 0.4$ (figure 2 of Bestion *et al.* 1983). Re_w is about 10 and a_w is about 0.4 in the present experiments. L should change less in this case. The hot-wire probe is not calibrated and L is assumed equal to 0.25. Re_w values in the free stream and at the maximum of pulsations in the boundary layer are close because this maximum is located near the edge of boundary layer at hypersonic speeds, which means that L values should be close at these locations and should not have a big influence on the receptivity coefficients obtained.

A temporal discrete Fourier transform is used to determine the amplitude (A) and phase (Φ) of controlled disturbances:

$$A(X,Y,Z)\exp(\mathrm{i}\Phi(X,Y,Z)) = \frac{2}{N}\sum_{j=1}^{N}\langle m\rangle(X,Y,Z,t_j)\exp(-\mathrm{i}wt_j)$$

where N is number of samples in a time series and, $\langle m\rangle$ the fluctuating part of an anemometer output signal.

To obtain the spatial wave spectra, discrete Fourier transforms with respect to the X-, Y-, Z-coordinates using a spectral window are used. The spectral windows are used to suppress the side lobes in spectral estimates, though this results in some degradation of spectral resolution (Marple 1987). The Kaiser–Bessel window is used in the present work:

$$W(\psi) = \frac{I_0(\pi k(1-(\psi/\Psi)^2)^{1/2})}{I_0(\pi k)}, \quad -\Psi \leqslant \psi \leqslant \Psi,$$

where $I_0(\xi) = \sum_{k=0}^{\infty}[(\xi/2)^k/k!]^2$ is a modified zero-order Bessel function.

For instance, the spectrum with respect to the spanwise wavenumber β is found from the following formula:

$$A(X,Y,\beta)\exp(\mathrm{i}\Phi(X,Y,\beta)) = \int_{-Z_0}^{Z_0} W(Z)A(X,Y,Z)\exp(\mathrm{i}\Phi(X,Y,Z))\exp(-\mathrm{i}\beta Z)\,\mathrm{d}Z.$$

Sometimes, due to an almost linear dependence of the disturbance phase on the X-coordinate, the wavenumber can be estimated from the formula: $\alpha = \Delta\Phi/\Delta X$.

3.1. *Acoustic radiation of a harmonic, moving source*

It is well known that a source of sound moving with a supersonic speed (V) generates acoustic disturbances propagating along Mach contours, and the vector of acoustic pulsations is directed perpendicular to these lines. The source with a harmonically varied amplitude will be called a harmonic source. The relationship between the longitudinal (α) and vertical (γ) wavenumbers of acoustic waves excited by a harmonic source with frequency f in a source-fixed coordinate system, is determined by the following formula:

$$\frac{\gamma}{(M_s^2-1)^{1/2}} = -\alpha + \frac{2\pi f_s}{V}\frac{M_s^2}{M_s^2-1} \tag{3.1}$$

where $M_s = V/a$.

Thus, we can obtain the inclination angle of the wave vector in the (X,Y)-plane:

$$\tan(\varphi) = \frac{\gamma}{\alpha} = (M_s^2-1)^{1/2}\left(-1+\frac{2\pi f_s}{\alpha V}\right). \tag{3.2}$$

In the general case, the phase velocity of acoustic waves is not related to the velocity of motion of the harmonic source. We pass now to the model-fixed coordinate system:

$$M_s = M(1 - W/U), \qquad f = f_s + \frac{W\alpha}{2\pi}$$

where $W = U - V$. In this coordinate system, a Doppler shift of the signal frequency occurs. For typical values of α obtained in this work, the Doppler shift should be observed even for a moderate velocity of the source. For example, a 1% shift of frequency occurs for $\alpha = 0.1$ and $1\,\mathrm{rad\,mm^{-1}}$ when $W = 31$ and $3.1\,\mathrm{m\,s^{-1}}$, respectively. No changes in pulsation frequency were observed in the experiments conducted. There is no Doppler shift if $f_s = 0$ or $W = 0$ and we will consider these cases in more detail.

The characteristics of a moving sources with constant amplitude ($f_s = 0$) can be found, for instance, in Laufer (1961). The phase velocity of acoustic waves (C) equals the velocity of motion (W) of the moving source with constant amplitude exciting these waves, the frequency of acoustic waves is determined by the formula $f = W\alpha/2\pi$. From (3.2) we obtain that

$$\tan(\varphi) = -(M_s^2 - 1)^{1/2} = -(M^2(1 - C/U)^2 - 1)^{1/2}. \tag{3.3}$$

This formula shows that the wave vector is directed perpendicular to Mach contours along which the acoustic disturbances propagate:

$$\tan(\psi) = 1/(M_s^2 - 1)^{1/2} = 1/(M^2(1 - C/U)^2 - 1)^{1/2} \tag{3.4}$$

where ψ is the inclination angle of Mach contours. From (3.3) we can obtain the relationship between the longitudinal (α) and vertical (γ) wavenumbers of acoustic waves generated by a moving source with constant amplitude:

$$\gamma = -\alpha(M^2(1 - C/U)^2 - 1)^{1/2}. \tag{3.5}$$

A moving source generates acoustic waves if it moves at a supersonic speed with respect to the flow velocity ($W/U < 1 - 1/M$ or $W/U > 1 + 1/M$).

Similar relationships can be also obtained for a motionless ($W = 0$) harmonic source:

$$\tan(\varphi) = -(M^2 - 1)^{1/2}(1 - C/U), \tag{3.6}$$

$$\tan(\psi) = 1/(M^2 - 1), \tag{3.7}$$

$$\gamma = -\alpha(M^2 - 1)^{1/2}\left(1 - \frac{C}{U}\frac{M^2}{M^2 - 1}\right). \tag{3.8}$$

The hot-wire probe whose wire is perpendicular to the velocity vector is sensitive to fluctuations of the longitudinal component of the mass flow. The relationship between the density and velocity fluctuations in an acoustic wave can be found from the mass-flow conservation equation in the direction of acoustic pulsations:

$$\frac{\rho'}{\rho} = -\frac{w'}{a} = -\frac{Mw'}{U},$$

where a is the speed of sound, w' are velocity fluctuations in an acoustic wave.

From this formula we can obtain the fluctuations of the longitudinal (u') and vertical (v') velocities:

$$\frac{u'}{U} = -\frac{\sin(\psi)}{M}\frac{\rho'}{\rho}, \qquad \frac{v'}{U} = -\frac{\cos(\psi)}{M}\frac{\rho'}{\rho}. \tag{3.9}$$

It is seen from these formulas that velocity fluctuations (w'/U) in an acoustic wave in a supersonic flow are smaller than density fluctuations (ρ'/ρ) by M times, and we can assume the hot-wire probe to be sensitive only to density fluctuations when acoustic disturbances are measured in a hypersonic flow. The longitudinal velocity fluctuations for a moving sources with constant amplitude

$$\frac{u'}{U} = -\frac{1}{M^2(1 - C/U)}\frac{\rho'}{\rho}$$

are the largest when $C/U = 1 \pm 1/M$ and equal to

$$\frac{u'}{U} = \mp\frac{1}{M}\frac{\rho'}{\rho}$$

in this case.

For a motionless harmonic source:

$$\frac{u'}{U} = -\frac{1}{M^2}\frac{\rho'}{\rho}, \qquad \frac{v'}{U} = -\frac{1}{M}\left(\frac{M^2 - 1}{M^2}\right)^{1/2}\frac{\rho'}{\rho}.$$

Finally, it can be noted that the most important characteristic of acoustic waves from the standpoint of receptivity is the direction of acoustic pulsations. The maximum receptivity can be expected for the radiation from a source with constant amplitude moving with velocity $1 \pm 1/M$, since in this case the acoustic pulsations are directed parallel to the flow and the longitudinal phase velocities of acoustic waves and Tollmien–Schlichting waves are equal.

4. Measurement results

4.1. *Mean flow parameters*

Flow over the test model can be divided in two areas: a weak interaction region with shock layer and a boundary layer region. The region of weak viscous interaction is situated at $0.3 < \bar{\chi} < 4$ (see for example Hayes & Probstein 1959), where $\bar{\chi}$ is the hypersonic interaction parameter. This parameter for a flat plate can be found by the formula: $\bar{\chi} = M_\infty^3(C_\infty/Re_\infty)^{1/2}$, where $C_\infty = (\mu_w T_\infty)/(\mu_\infty T_w)$; μ is dynamic viscosity, index w indicates parameters at the wall. For the conditions of the present experiments the weak interaction region is situated at $0.2\,\text{mm} < X < 33\,\text{mm}$. The displacement effect caused by the thick boundary layer results in the appearing of the bow shock at hypersonic speeds even on the flat plate with a sharp leading edge. Also, the weak interaction region can be characterized by a favourable induced pressure gradient rapidly moving downstream.

To determine the mean parameters of the boundary layer on the test model, measurements are performed by a flattened Pitot tube (the tube height was 0.25 mm). Figure 4 shows the measured results for the mean parameters of the boundary layer as functions of the Mach number M/M_∞ and velocity U/U_∞, normalized to the corresponding free-stream values, versus the Blasius coordinate, $\eta = Y(Re_1/X)^{1/2}$. The Mach number distributions are obtained using the Rayleigh formula and the measured values of static and Pitot pressures. A modified Crocco integral for a laminar boundary layer and adiabatic wall conditions is used to calculate the velocity: $T/T_\infty = 1 + 0.5(k-1)(Pr)^{1/2}M_\infty^2(1 - (U/U_\infty)^2)$, where $k = 1.4$ is specific heat ratio, Pr is Prandtl number. The curves plot the results obtained from the computation of compressible boundary layer equations, symbols show the experimental data obtained for different longitudinal coordinates.

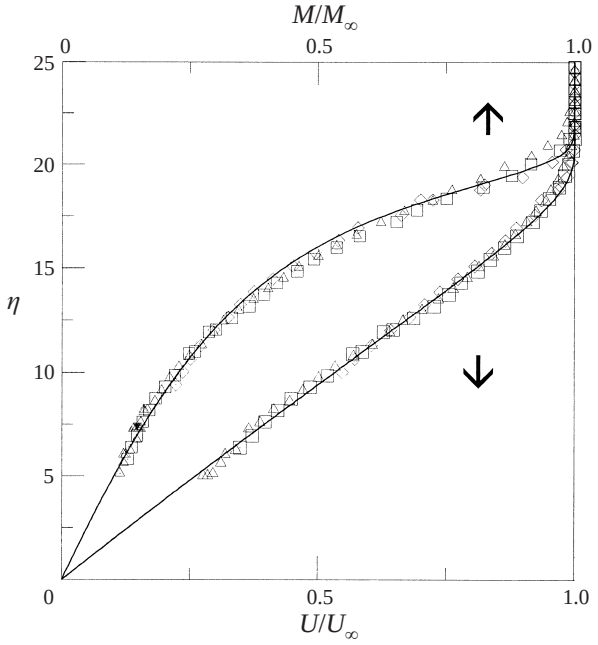

FIGURE 4. Normalized Mach number M/M_∞ and velocity U/U_∞ versus Blasius coordinate: ———, calculation from compressible boundary layer equations; ◇, $X = 96$ mm; □, 121; △, 138.

The boundary layer thicknesses at the measured cross-sections shown in figure 4 are about 1.8, 2.0, 2.2 mm, respectively. Errors of momentum thickness displacement caused by the thick Pitot tube do not exceed 3% at the first measured cross-section according to Monaghan (1957). Errors in the displacement thickness and shape factor calculated using experimental profiles do not exceed 2% and 1% respectively compared with theoretical ones. Such precision satisfies Saric's requirements. This testifies that a gradientless flow with a self-similar boundary layer is obtained on the test model in the experiments.

4.2. *Acoustic waves in the free stream*

The distributions of pulsation amplitudes and phases along the longitudinal coordinate X_1 are presented in figure 5(a, b) for three-dimensional and in figure 5(c) for two-dimensional perturbers, in the symmetry plane of the model ($Z_1 = 0$) for $Y_1 = 13.6$, 10.8, 18.8 mm and peak voltage on the electrodes $E = 600$, 700, 700 V for each of three variants, respectively. A is the amplitude of mass-flow fluctuations normalized to the value of mass flow in free stream. In phase distributions, one can roughly see typical zones of disturbances with a constant phase velocity on the basis of linear sections of phase variation along X_1.

The distributions in figure 5(a) consist of a few amplitude peaks and a few parts with constant phase slope. Such a distributions are very similar to data obtained in Semionov *et al.* (1996) and Kosinov *et al.* (1996). In these works, the disturbances were introduced by local glow discharge through an aperture in the model surface. The static pressure is much less in our experiments and equals 740 Pa. The discharge behaviour under increasing voltage is observed through the test section window. At low voltages on the electrodes, $E \approx 600$ V (figure 5a), a glow discharge introduces local disturbances through an orifice in the plate. In this case, the mechanism of

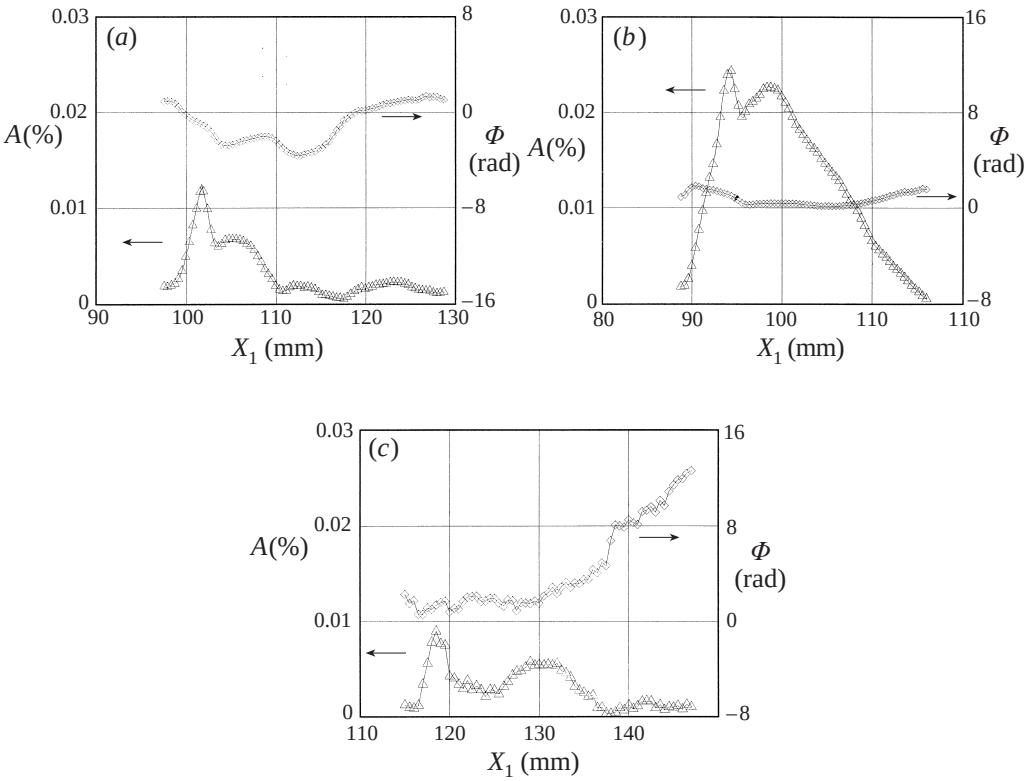

FIGURE 5. Amplitude (△) and phase (◇) of pulsations in the free stream along the streamwise coordinate X_1; $Z_1 = 0$: three-dimensional perturber (*a*) $Y_1 = 13.6$ mm, $E = 600$ V, (*b*) $Y_1 = 10.8$ mm, $E = 700$ V, (*c*) two-dimensional perturber, $Y_1 = 18.8$ mm, $E = 700$ V.

introducing disturbances is, apparently, the same as that described in Kosinov *et al.* (1996), i.e. there is an injection-suction mechanism, and a horseshoe vortex generating acoustic and Tollmien–Schlichting waves is formed on the model surface.

As the voltage on the electrodes is increased up to $E \approx 700$ V, a glowing discharge appears on the model surface, its size increasing with increasing voltage. Glowing in the form of a flat streamwise-extended oval is observed. Glowing in the orifice is also observed, which indicates the presence of a glow discharge there too. The results of observation are consistent with the measurement data. A comparison of figure 5(*a*) and 5(*b*), shows that the size of the disturbed zone increases by a factor of two. This is due to an increase of the glowing discharge size on the surface with increasing voltage. At the same time, a peak of the disturbances amplitude introduced by a glow discharge in the aperture can be identified in both figures. When there are these two glowing discharges, the mechanism of disturbance introduction is more complicated. The glow discharge in aperture introduces disturbances through the injection-suction mechanism described above. The glow discharge on the surface produces thermal energy in a zone of length approximately 40 boundary layer thicknesses. From the viewpoint of introducing acoustic waves into the flow, the glowing discharge on the surface is an analogue of a large vibrating membrane.

The amplitude and phase distributions of pulsations along the longitudinal co-ordinate for a two-dimensional perturber (figure 5*c*) are similar to the plots for a

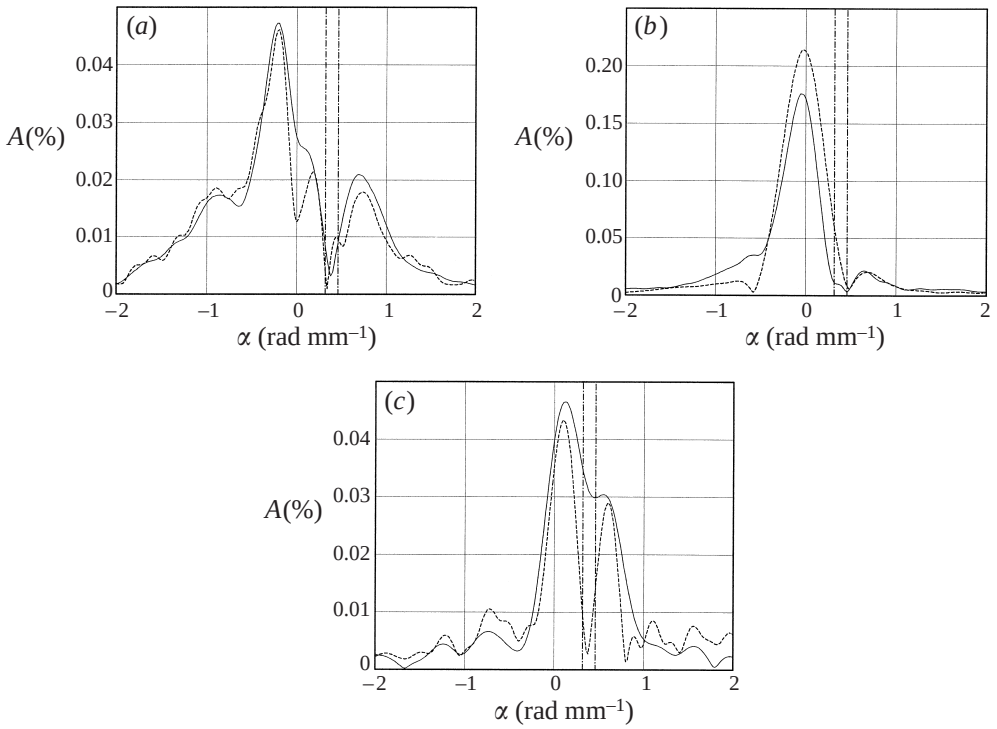

FIGURE 6. α-spectra: three-dimensional perturber (*a*) $Y_1 = 13.6\,\text{mm}$, $E = 600\,\text{V}$, (*b*) $Y_1 = 10.8\,\text{mm}$, $E = 700\,\text{V}$, (*c*) two-dimensional perturber $Y_1 = 18.8\,\text{mm}$, $E = 700\,\text{V}$; ———, Kaiser–Bessel spectral window; – – – –, without window; — · —, $C = 1 \pm 1/M_\infty$.

three-dimensional perturber. However, the zone of negative phase velocities is almost absent.

From the standpoint of introducing acoustic radiation, a disturbance in the boundary layer can be represented as a set of point sources of acoustic waves whose characteristics were considered above (§ 3.1), and the acoustic field in the free stream is the result of interference of these waves.

Figure 6 shows the α-spectra obtained using a discrete Fourier transformation of the data shown in figure 5. The solid curves show the data obtained using the Kaiser–Bessel window; the dashed curves show the data obtained without a spectral window. The dash-dotted lines show the values of α for which the phase velocity with respect to the flow is equal to the speed of sound.

It is seen from these plots that the α-spectrum consists of several peaks, and each of them corresponds to a particular zone of radiation in the distributions in figure 5. The largest amplitudes of acoustic radiation are observed when α is close to zero, and correspond to the zone of glow discharge in the X_1 distributions (figure 5). For these values of α the phase velocity is significantly larger than the flow velocity. Acoustic waves with these phase velocities can be generated only by motionless harmonic sources because their phase velocity depends only on the phase difference between the sources and can be arbitrary. For example, if there is no phase difference between the motionless harmonic sources the phase velocity of generated acoustic waves is infinitely large. A minimum in the amplitude of acoustic radiation is observed in the region of subsonic disturbances (the region bounded by dash-dotted lines). Another

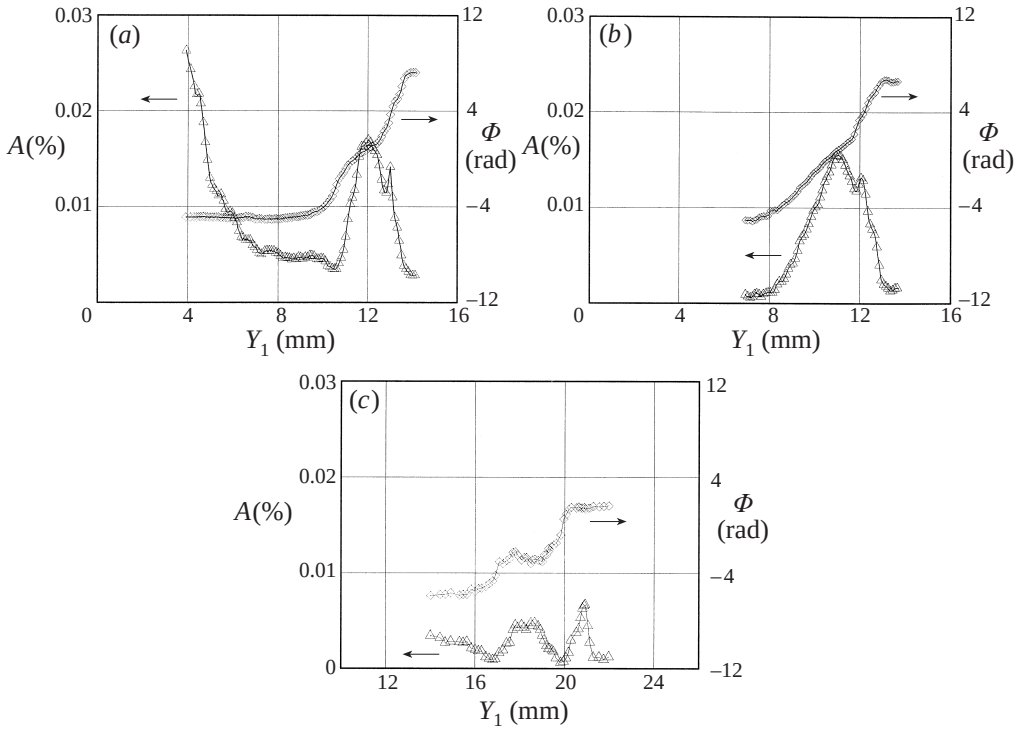

FIGURE 7. Amplitude (△) and phase (◇) of pulsations in the free stream along the coordinate Y_1; $Z_1 = 0$: three-dimensional perturber $X_1 = 99$ mm, (*a*) $E = 600$ V, (*b*) $E = 700$ V, (*c*) two-dimensional perturber $X_1 = 132.5$ mm, $E = 700$ V.

maximum of radiation is observed at $\alpha \approx 0.65\,\mathrm{rad\,mm^{-1}}$ ($C/U \approx 0.59 < 1 - 1/M_\infty$). In the X_1 distributions (figure 5) this peak corresponds to the radiation from a region located downstream from the discharge. Extrapolation of the phase velocity of acoustic radiation in the test section of a supersonic wind tunnel, which was obtained in the Mach number range $M_\infty = 2$–5 in Laufer (1964) and Lebiga & Zinoviev (1997), yields the phase velocity $C/U \approx 0.58$ for $M_\infty = 6$, which is close to the value of the phase velocity in the second peak. The sources of these acoustic waves are vortices moving in the boundary layer, which are moving sources with constant amplitude of radiated acoustic waves.

A comparison of figures 6(*a*) and 6(*b*) shows that an increase of voltage on the three-dimensional perturber leads to an increase of radiation for $\alpha \approx 0$, whereas the radiation in the second peak from moving sources with constant amplitude does not change. The value of the second peak is maximum in the α-spectrum of the two-dimensional source (figure 6*c*); this source is the most effective for generating moving vortices in the boundary layer.

Figure 7 shows the amplitude and phase distributions of pulsations along the vertical coordinate Y_1 in the symmetry plane of the model ($Z_1 = 0$) for each of the three variants. The pulsation amplitude distributions along Y_1 are in qualitative agreement with the distributions along X_1 in the zone of the maximum. When approaching the wall, the amplitude of pulsations significantly increases. The phase of pulsations changes strongly in the region of maximum pulsations from the source and then it is nearly constant when approaching the model.

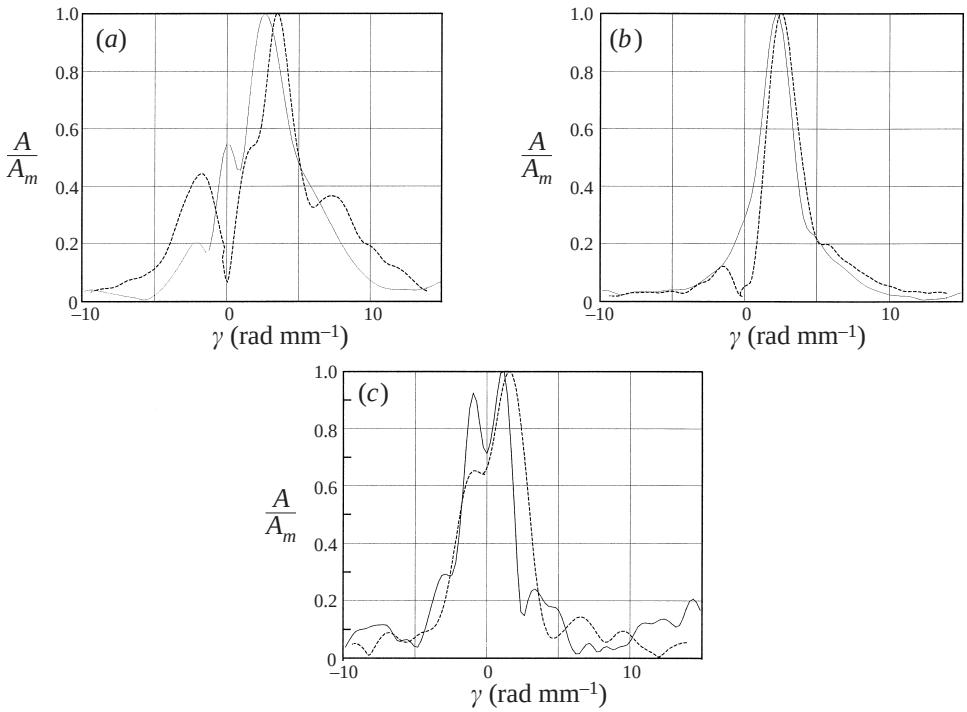

FIGURE 8. γ-spectra: three-dimensional perturber $X_1 = 99$ mm, (*a*) $E = 600$ V, (*b*) $E = 700$ V, (*c*) two-dimensional perturber $X_1 = 132.5$ mm, $E = 700$ V; ——, γ; – – – –, $\gamma = f(\alpha)$.

Using a discrete Fourier transformation along Y_1, γ-spectra are obtained. These spectra are shown as solid curves in figure 8. The γ-spectra consist of one (figure 8*b*) or two (figure 8*a*, *c*) large peaks and several small peaks close to them, which cannot be resolved by a usual Fourier transformation. Using equations (3.5), (3.8), we can estimate the γ-spectra on the basis of the α-spectra. The results of these estimates are shown by the dashed lines in figure 8. A reasonable agreement of results obtained verifies that the artificial disturbances of the free stream are acoustic waves.

In this case, we can estimate the inclination angles of the wave vectors φ and Mach contours ψ in the free stream using formulas (3.3), (3.4), (3.6), (3.7). The results of such an estimate are presented as the amplitude of radiation versus the wave inclination angle φ in figure 9(*a*) and ψ in figure 9(*b*). It can be noted that the waves of large amplitude are introduced at $\varphi \approx 90°$, $\psi \approx 9.7°$, and the second peak of radiation corresponds to the angles $\varphi \approx 115°$ and $\psi \approx 25°$.

Examples of distributions of pulsation amplitudes and phases over the transverse coordinate Z_1 for a three-dimensional and two-dimensional sources of disturbances are shown in figure 10. The Z_1 distributions of amplitudes and phases for a three-dimensional source are not completely symmetrical, which is caused by discharge asymmetry. Measured Z_1 distributions for different X_1 are similar. The transverse distributions of disturbances radiated by two-dimensional source are measured only partially because of traverse gear limitations. The amplitudes and phases of acoustic waves from a two-dimensional source are almost constant in the Z_1-direction over the measured distance. Glowing over electrodes was uniform; therefore amplitude and phase should be close to constant over the full distance.

From a discrete Fourier transformation of the Z_1 distributions we obtain β-spectra

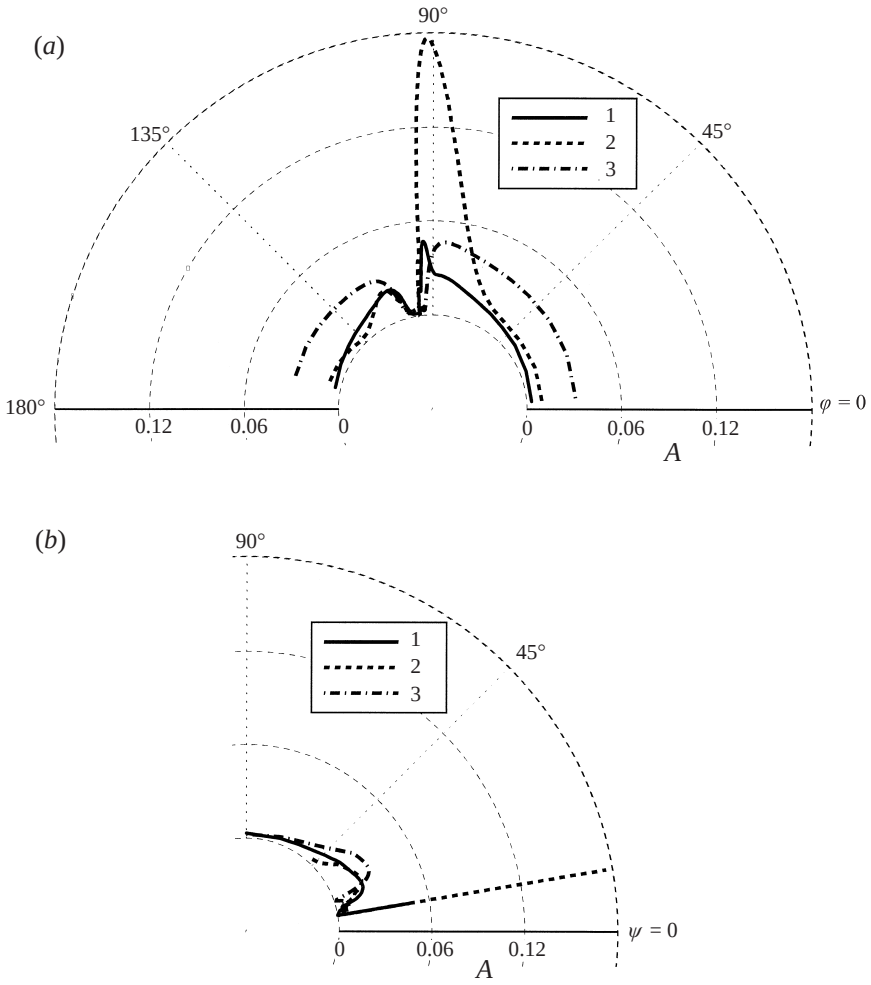

FIGURE 9. Amplitude of acoustic radiation (A) versus φ (a) and ψ (b): three-dimensional perturber curve 1, $E = 600\,\mathrm{V}$; 2, $E = 700\,\mathrm{V}$; 3, two-dimensional perturber, $E = 700\,\mathrm{V}$.

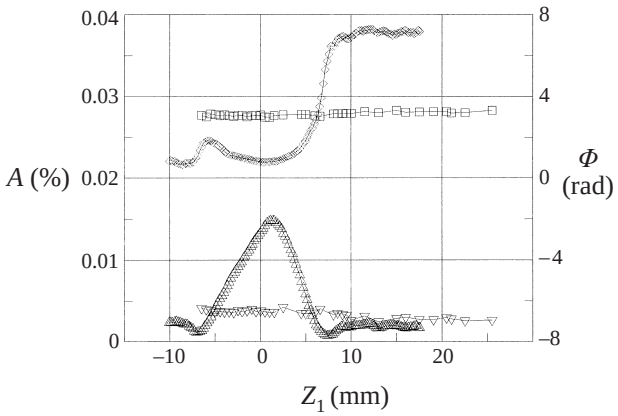

FIGURE 10. Amplitude ($\triangle$, $\triangledown$) and phase ($\diamond$, $\square$) distributions along the transverse coordinate for three-dimensional and two-dimensional perturbers respectively.

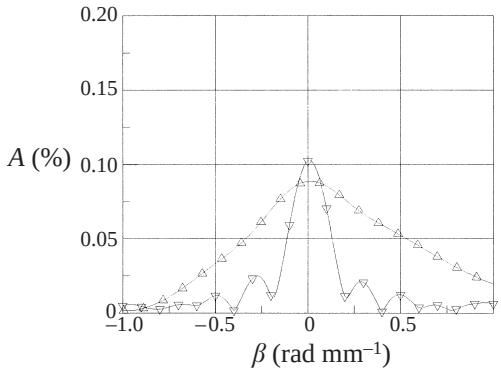

FIGURE 11. β-spectra for three-dimensional ($\triangle$) and two-dimensional ($\triangledown$) perturbers.

for three-dimensional and two-dimensional sources of disturbances (figure 11). The spectra for a three-dimensional source are similar to the results of Semionov *et al.* (1996) and Kosinov *et al.* (1996). Phase β-spectra for different X_1 are also similar, it means that C is about the same for all β. This is in agreement with other publications (see, for example, Maslov, Shiplyuk & Sidorenko 1997) where it was found that C of artificial disturbances from a three-dimensional perturber is constant within 10% for all wave inclination angles. The amplitude β-spectrum for two-dimensional source has a narrow peak near zero. It means that this source emits plane acoustic waves. Small additional peaks appear because of the limited measured distance in the Z_1-direction.

4.3. *Measurements of receptivity*

For receptivity measurements the test model is placed on a pylon, and experiments with two models are performed (see figure 2). To achieve the maximum accuracy of results, it was decided to perform all necessary measurements during one run. In this case, we have to measure the X and Z distributions of pulsations in the incoming flow at the leading edge of the test model and the same distributions in the boundary layer on the test model in order to obtain the α- and β-spectra of external acoustic disturbances and disturbances of the boundary layer. Three measurements of this type with the three-dimensional perturber are performed at $E = 600$ V, $\Delta Y = 11.6$ and 10.8 mm; $E = 700$ V, $\Delta Y = 12.4$ mm. Two measurements are performed with the two-dimensional perturber: $E = 700$ V, $\Delta Y = 17.3$ and 20.3 mm. The X distributions upstream of the leading edge of the test model are measured at $Y = 0.4$ mm, $Z = 0$ up to the intersection with the bow shock wave; the Z distributions are measured at $X = 0$, $Y = 0.4$ mm.

The boundary layer measurements are performed in a standard manner in the layer of maximum pulsations. For this purpose the maximum of pulsations is found in the boundary layer, the mean voltage on the hot-wire probe is measured, then the probe is moved in the X- or Z-directions and the Y-coordinate of the probe is set so that the mean voltage on the hot-wire probe is kept constant. In this case, the probe motion takes place in the layer with constant mean flow parameters.

Knowing the variation of pulsation phases in the X-direction in the centre of the wave train, we can evaluate the longitudinal wavenumber α and the phase velocity in the X-direction C. A polynomial approximation is used to find the phase derivative of external acoustic disturbances with respect to X. The following values of the longitudinal wavenumber are obtained for the three-dimensional perturber: $\alpha = -0.51$,

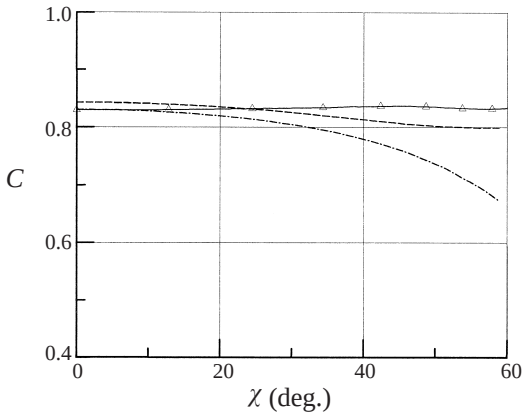

FIGURE 12. Dependence C on χ. $\triangle$, experiment; – – – –, local parallel stability theory; —·—, $C = 1 \pm 1/M_\infty \cos(\chi)$.

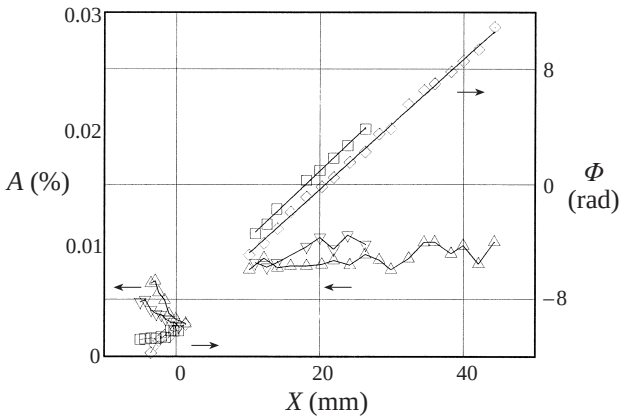

FIGURE 13. Amplitude ($\triangle$, $\triangledown$) and phase ($\diamond$, $\square$) distributions along X in the free stream near the leading edge and in the boundary layer for a two-dimensional perturber at $\Delta Y = 17.3$ and 20.3 mm, respectively.

0.21, $-0.26\,\mathrm{rad\,min^{-1}}$. The normalized longitudinal phase velocities calculated on the basis of these values of α are $C/U = -0.75, 1.83, -1.48$. This means that the leading edge experiences the influence of radiation from a motionless harmonic source. Using formulas (3.6), (3.7) we can estimate the inclination angles of the acoustic wave in the (X, Y)-plane: $\varphi = 84, 102, 86^\circ$ and $\psi = 9.7^\circ$.

The measurement of phase distributions along X in the boundary layer shows that the phase changes linearly. Using the phase β-spectra, the longitudinal phase velocity is obtained (figure 12). The value of the phase velocity is close to the phase velocity of the Tollmien–Schlichting waves calculated by local parallel stability theory, hence the acoustic waves generate the Tollmien–Schlichting waves in the boundary layer.

The amplitude and phase distributions of pulsations along the X-coordinate for a two-dimensional perturber in the free stream near the leading edge and in the boundary layer for the maximum of pulsations are shown in figure 13. In the first distribution ($\Delta Y = 17.3\,\mathrm{mm}$) the waves have the following parameters at the leading edge: $\alpha \approx 0.6\,\mathrm{rad\,mm^{-1}}$, $C/U \approx 0.64$. In this case, acoustic waves from a moving source with constant amplitude fall onto the leading edge, and the wave

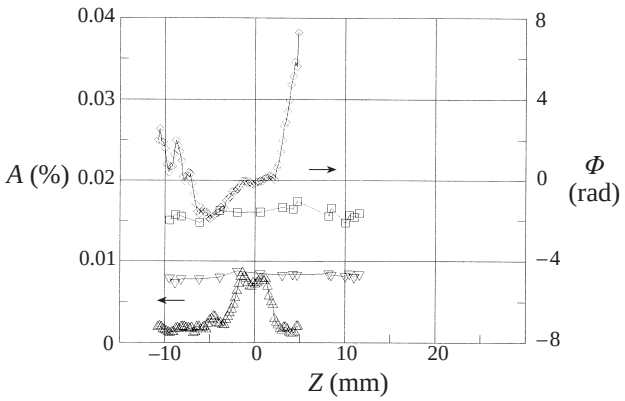

FIGURE 14. Amplitude (△, ▽) and phase (◇, □) distributions along the transverse coordinate in the boundary layer for three-dimensional and two-dimensional perturbers respectively.

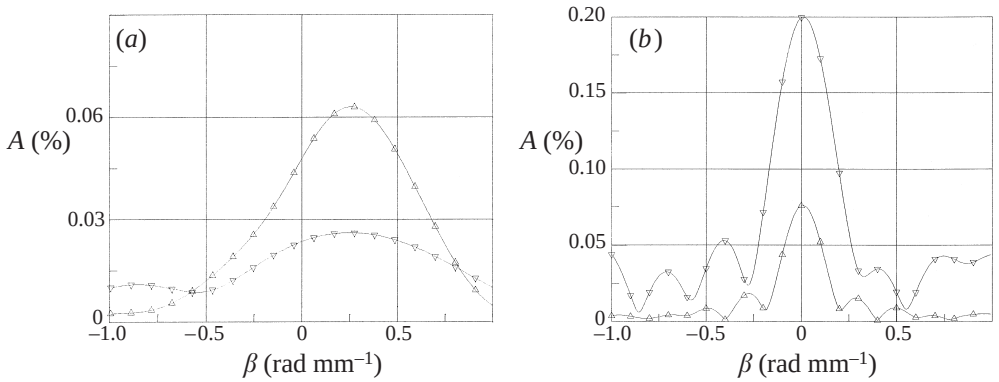

FIGURE 15. β-spectra in the free stream near the leading edge (△) and in the boundary layer (▽) for three-dimensional (*a*) and two-dimensional (*b*) perturbers.

inclination angles calculated by formulas (3.3), (3.4) are $\varphi = 118°$ and $\psi = 28°$. Unfortunately, the number of samples and the measurement accuracy are not sufficient to determine the longitudinal wavenumber of the free-stream disturbances in the second distribution. The phase distributions along X in the boundary layer are linear. The following wave characteristics of disturbances are obtained in the boundary layer: $\alpha = 0.45, 0.47\ \mathrm{rad\,mm^{-1}}$, $C/U = 0.85, 0.82$ for the first and second distributions, respectively, i.e. Tollmien–Schlichting waves are excited in the boundary layer. The amplitude of pulsations in the boundary layer weakly increases with increasing X-coordinate.

The distributions of pulsation amplitudes and phases over the transverse coordinate, measured in the boundary layer on the test model in the case of three-dimensional and two-dimensional perturbers (figure 14) and β-spectra (figure 15) are similar to the profiles obtained when the pulsation fields are measured in the free stream (they are shown in figures 10, 11).

From a discrete Fourier transformation of the Z distributions for three-dimensional and two-dimensional perturbers, β-spectra are obtained. As an example, figure 15 shows the β-spectra of pulsations in the external flow and in the boundary layer, which are measured in one run, for three-dimensional and two-dimensional sources

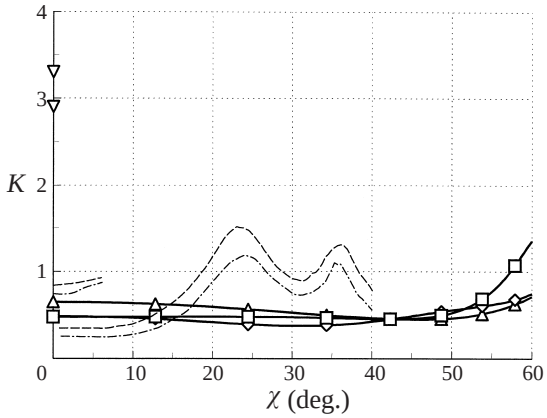

FIGURE 16. Receptivity coefficients versus wave inclination angle for three-dimensional (△, ◇, □) and two-dimensional (▽) perturbers. Data of Semionov *et al.* (1996) for $M = 2$: – – – –, $X_1 = 40$ mm; — · —, 50.

respectively. It is seen that for a three-dimensional source the maxima of pulsations in the external flow and in the boundary layer lie at $\beta = 0.25\,\mathrm{rad\,mm^{-1}}$. The amplitude of pulsations in the boundary layer for $|\beta| < 0.7\,\mathrm{rad\,mm^{-1}}$ is smaller than in the external flow. For $|\beta| > 0.7\,\mathrm{rad\,mm^{-1}}$ the amplitude of pulsations in the boundary layer becomes larger than in the external flow. Unlike three-dimensional source data, pulsations in the boundary layer for a two-dimensional source are higher than in the free stream. The narrow peak at zero shows that two-dimensional acoustic waves excite waves with $\chi = 0$ in the boundary layer.

The boundary layer measurements are carried out for different longitudinal coordinate X, and for comparison purposes the β-spectra are recalculated on the basis of the local-parallel theory of stability to the lower branch of the neutral curve $X = X_N$.

Since the amplitudes of controlled mass flow fluctuations are very small in the experiments (less than 0.04%), we can consider the boundary layer receptivity on the leading edge of the model to external acoustic disturbances as a linear process. The receptivity coefficient can be determined as

$$K(\beta) = \frac{A(\beta)_{X=X_N}}{A(\beta)_{X=0}}.$$

The receptivity coefficients for all measurements, which are calculated using the above formula, are shown in figure 16 as functions of the wave inclination angle χ. Only positive angles χ are plotted. The presented receptivity coefficients are averaged over the positive and negative inclination angles $K = (K_{\chi<0} + K_{\chi>0})/2$. Although β-spectra (figure 15) are asymmetric, $K_{\chi<0} \approx K_{\chi>0}$. For disturbances from a three-dimensional perturber, the receptivity coefficients for the wave inclination angle $\chi = 0^\circ$ are $K \approx 0.57$. As χ increases, the receptivity coefficients slightly decrease down to $K \approx 0.46$ for $\chi = 35$–48°, and then rapidly increase up to $K \approx 1.0$ for $\chi = 60^\circ$. Unfortunately we do not have an exact explanation of the increase that occurs near $\chi \approx 55^\circ$. One possible reason is the increase of measurements error at high angles because of the worsening signal/noise ratio. K obtained at different amplitude levels of external acoustic waves are found to be the same in the limit of experimental errors. This confirms that the receptivity process under consideration is linear.

The receptivity coefficients for disturbances from a two-dimensional perturber are equal to 2.9 and 3.3 for the first and second distribution, respectively.

After finding this great difference in receptivity for three-dimensional and two-dimensional perturbers we tried to get higher receptivity for acoustic waves radiated by a three-dimensional perturber. To do that the measurements are carried out at different ΔY. Additionally, the voltage on the electrodes is changed during a run and the signal on the hot wire is monitored when probe is positioned in the boundary layer of the test model at the middle of the generated wave packets. But all attempts failed because the receptivity coefficients do not change. In our opinion the most likely explanation of the difference in receptivity coefficients for three-dimensional and two-dimensional perturbers is that in the first case the receptivity to acoustic waves with a small inclination angle ψ generated by harmonic motionless sources is investigated, whereas in the second it is the receptivity to acoustic waves with larger inclination angles from moving sources with constant amplitude. It is shown above that wave characteristics of acoustic radiation from moving sources with constant amplitude produced by artificial perturbers are the same as the characteristics of radiation of a turbulent boundary layer on nozzle walls. This means that the coefficients obtained for a two-dimensional perturber should be used for determination of receptivity to acoustic waves in wind tunnels.

Coefficients for disturbances from a two-dimensional perturber are approximately 5 to 6 times larger than the above coefficients of receptivity to disturbances from a three-dimensional perturber at zero angle χ, and approximately 4 times larger than those obtained at $M_\infty = 2$ in Semionov *et al.* (1996) (figure 16). In that work it was not described what kind of disturbances was generated in the boundary layer and receptivity coefficients were obtained in arbitrary position. So it is difficult to make reliable quantitative comparison of the receptivity coefficients for $M_\infty = 2$ and $M_\infty = 6$.

5. Conclusions

The receptivity of the boundary layer on the leading edge of a flat plate to controlled acoustic disturbances with frequency of 50 kHz ($F = 0.30 \times 10^{-4}$) from three-dimensional and two-dimensional perturbers is experimentally studied for the free-stream Mach number $M_\infty = 5.92$ and unit Reynolds number $Re_1 = 13 \times 10^6\ \mathrm{m}^{-1}$.

The spatial field of the free-stream controlled disturbances is studied. The resultant spatial distributions of pulsations excited by a three-dimensional perturber are similar to data measured at $M_\infty = 2$ and 3.5. It is shown that the perturbers generate acoustic waves in the free stream. The acoustic radiation can be presented as the radiation from motionless harmonic sources and from moving sources with constant amplitude. It is found that acoustic waves incident onto the leading edge excite Tollmien–Schlichting waves in the boundary layer. The receptivity coefficients depend on the inclination angles of incident acoustic waves.

A comparison of receptivity coefficients obtained for $M_\infty = 6$ with the results of Semionov *et al.* (1996) ($M_\infty = 2$) and Kosinov *et al.* (1996) ($M_\infty = 3.5$) shows that the boundary layer receptivity to external acoustic disturbances increases as the Mach number increases.

This work was supported by CERT ONERA, contract No. 11480/96 and RFBR, grant 98-01-00735.

REFERENCES

Bestion, D., Gaviglio, J. & Bonnet, J. P. 1983 Comparison between constant-current and constant-temperature hot-wire anemometers in high-speed flows. *Rev. Sci. Instrum.* **54**, 1513–1524.

Choudhari, M. & Streett, C. 1990 Boundary layer receptivity phenomena in three-dimensional and high-speed boundary layers. *AIAA Paper* 90-5258.

Duck, P. W., Lasseigne, D. G. & Hussaini, M. Y. 1997 The effect of three-dimensional freestream disturbances on the supersonic flow past a wedge. *Phys. Fluids* A **2**, 456–467.

Fedorov, A. V. & Khohlov, A. P. 1993 Excitation and evolution of unstable disturbances in supersonic boundary layer. *Proc. 1993 ASME Fluid Engineering Conference, Washington, DC*. FED-Vol. 151, *Transitional and Turbulent Compressible Flows*, pp. 1–13.

Gaponov, S. A. 1977 Interaction of a supersonic boundary layer with acoustic disturbances. *Izv. Akad. Nauk USSR. Zh. Mech. Zhidk. i Gaza* **6**, 51–56 (in Russian).

Gaponov, S. A. 1995 On the interaction of a supersonic boundary layer with acoustic waves. *J. Thermophys. Aeromech.* **3**, 181–189.

Goldstein, M. E. & Hultgren, L. S. 1989 Boundary-layer receptivity to long-wave free-stream disturbances. *Ann. Rev. Fluid Mech.* **21**, 137–166.

Grigoriev, V. D., Klemenkov, G. P., Omelaev, A. I. & Kharitonov, A. M. 1972 Hypersonic wind tunnel T-326. In *Aerofizicheskie Issledovania* (ed. A. M. Kharitonov), pp. 16–18. Novosibirsk (in Russian).

Hayes, W. D. & Probstein, R. F. 1959 *Hypersonic Flow Theory*. Academic.

Kachanov, Yu. S., Kozlov, V. V. & Levchenko, V. Ya. 1981 *Beginning of Turbulence in a Boundary Layer*. Novosibirsk: Nauka (in Russian).

Kendall, J. M. 1967 Supersonic boundary layer stability experiments. *Aerospace Rep.* TR-158 (S3816-63)-1, Vol. 2, pp. 10-1–10-8.

Kendall, J. M. 1975 Wind tunnel experiments relating to supersonic and hypersonic boundary-layer transition. *AIAA J.* **13**, 290–299.

Kendall, J. M. 1990 Boundary layer receptivity to freestream turbulence. *AIAA Paper* 90-1504.

Kerschen, E. J. 1989 Boundary layer receptivity. *AIAA Paper* 89-1109.

Kosinov, A. D., Maslov, A. A. & Semionov, N. V. 1996 Modified method of experimental study of supersonic boundary layer receptivity. *Intl Conf. on Methods of Aerophysical Research, Novosibirsk*, pt.3, pp. 161–166. Novosibirsk.

Kosinov, A. D., Maslov, A. A. & Shevelkov, S. G. 1990 Experiments on the stability of supersonic laminar boundary layers. *J. Fluid Mech.* **219,** 621–633.

Kovasznay, L. S. G. 1954 Hot-wire method. *High Speed Aerodynamic and Jet Propulsion*, Vol. **9**, pp. 219–285, Princeton University Press.

Kozlov, V. V. & Ryzhov, O. S. 1990 Asymptotic theory and experiment. *Proc. R. Soc. Lond.* A **429**, 341–373.

Laufer, J. 1961 Aerodynamic noise in supersonic wind tunnels. *J. Aero. Sci.* **9**, 685–692.

Laufer, J. 1964 Some statistical properties of the pressure field radiated by a turbulent boundary layer. *Phys. Fluids* **8**, 1191–1197.

Lebiga, V. A. & Zinoviev, V. N. 1997 Fluctuation characteristics of flows in test sections of high-speed wind tunnels. *AGARD-CP* 585, pp. 31-1–31-9.

Mack, L. M. 1975 Linear stability theory and the problem of supersonic boundary layer transition. *AIAA J.* **13**, 423–448.

Malik, M. R., Lin, R.-S., Sengupta, R. 1999 Computation of hypersonic boundary layer response to external disturbances. *AIAA Paper* 99-0411.

Marple, S. L. Jr 1987 *Digital Spectral Analysis with Application*. Prentice-Hall.

Maslov, A. A. & Semionov, N. V. 1986 Excitation of eigen boundary layer oscillations by external acoustic field. *Izv. Akad. Nauk USSR. Zh. Mech. Zhidk. i Gaza* **3**, 74–78 (in Russian).

Maslov, A. A. & Semionov, N. V. 1987 Acoustic disturbances and supersonic boundary layer. In *Problems of Nonlinear Acoustics*, pp. 132–134. Novosibirsk (in Russian).

Maslov, A. A., Shiplyuk, A. N. & Sidorenko, A. A. 1997 Study related to hypersonic boundary layer stability on a cone with a flare. Preprint/*RAS SB, ITAM* 2-97. Novosibirsk.

McKenzie, J. F. & Westphal, K. O. 1968 Interaction of linear waves with oblique shock waves. *Phys. Fluids* **11**, 2310–2332.

Monaghan, R. J. 1957 The use of Pitot tubes in the measurements of laminar boundary layers in supersonic flow. *ARC R. & M.* 3056.

Morkovin, M. V. 1969 Critical evaluation of transition from laminar to turbulent shear layers with emphasis on hypersonically traveling bodies. *AFFDL-TR* 68-149.

Nishioka, M. & Morkovin, M. V. 1986 Boundary-layer receptivity to unsteady pressure gradients: experiments and overview. *J. Fluid. Mech.* **171**, 219–262.

Saric, W. S. 1990 Low-speed experiments: requirements for stability measurements. In *Instability and Transition* (ed. M. Y. Hussaini & R. G. Voight), vol. 1, pp. 162–174. Springer.

Schmisseur, J. D., Schneider, S. P. & Collicott, S. H. 1998 Receptivity of the Mach-4 boundary-layer on an elliptic cone to laser-generated localized freestream disturbances. *AIAA Paper* 98-0532.

Semionov, N. V., Kosinov, A. D. & Maslov, A. A. 1996 Experimental investigation of supersonic boundary layer receptivity. *Proc. of Colloquium 'Transitional Boundary Layer in Aeronautics'*, pp. 413–420. North-Holland.

Zhong, X. 1997 Direct numerical simulation of hypersonic boundary layer transition over blunt leading edges, part 2: receptivity to sound. *AIAA Paper* 97-0756.